Wideband hysteresisgraph with digital feedback

S. Dobák[1]
[1]*Institute of Physics, Faculty of Science, P. J. Šafárik University in Košice, 04154 Košice, Slovakia*

(Dated: 15 August 2024)

Funded by the European Union's NextGenerationEU program through the Recovery and Resilience Plan for Slovakia under the Project No. 09I03-03-V04-00008.

As part of the project, a wideband hysteresisgraph-wattmeter was developed to enable fluxmetric measurements over the frequency range spanning from quasi-DC to 1 MHz. A schematic of the implemented fluxmetric measurement setup is shown in Fig. 1.

The N_1-turn magnetizing winding was excited by either a 10 MHz function/arbitrary waveform generator (Agilent 33210A) or a 160 MHz generator (Rigol 4162). The excitation signal was then amplified using a four-quadrant power amplifier Toellner TOE 7621, denoted as PA in Fig. 1. The voltage drop $u_H(t)$ across a calibrated non-inductive resistor R_H was measured to determine the magnetizing current via $i_H(t) = u_H(t)/R_H$. The voltage $u_2 = -N_2 A\mathrm{d}B/\mathrm{d}t$ induced in the secondary winding, often of very low amplitude, was suitably amplified. To mitigate potential phase shifts introduced by amplification—even when using high-quality amplifiers—both $u_H(t)$ and $u_2(t)$ were processed using identical low-noise DC-coupled preamplifiers (Stanford Research Systems SR560, labeled A in Fig. 1), typically configured with different gains.

The amplified signals were synchronously acquired and digitized using a 12-bit, 200 MHz, 2 GSa/s four-channel oscilloscope (Keysight 1204G), and subsequently processed by a PC running LabVIEW-based control software. Spurious coupling effects between the primary and secondary windings were minimized through optimized winding configuration, short connection leads, and frequency-dependent adjustment of turn counts. A photograph of the constructed setup is provided in Fig. 2.

The magnetic field strength applied to the sample is calculated as

$$H(t) = \frac{1}{G_H}\frac{\tilde{u}_H(t)}{R_H}\frac{N_1}{l_\mathrm{m}}, \tag{1}$$

where G_H is the gain of the preamplifier through which $u_H(t)$ was passed, $\tilde{u}_H(t)$ is the amplified voltage signal, and l_m is the magnetic path length of the sample.

The magnetic induction is numerically computed using the trapezoidal rule:

$$B(t) = \frac{1}{AN_2}\int \frac{1}{G_B}\tilde{u}_2(t)\,\mathrm{d}t, \tag{2}$$

where G_B denotes the gain of the preamplifier used to amplify $u_2(t)$ to $\tilde{u}_2(t)$.

The magnetic field $H(t)$ and the magnetic polarization $J(t) \approx B(t)$ define the dynamic hysteresis loop in the H–J plane, as illustrated in Fig. 3. A critical aspect of accurate hysteresis loop measurements is the precise definition of measurement conditions to ensure comparability. International standards prescribe a sinusoidal induction waveform for dynamic hysteresis loop characterization. However, due to the nonlinear behavior of magnetic materials—particularly at higher peak polarization levels J_p—a sinusoidal magnetic field excitation may result in a distorted $J(t)$ waveform. These considerations motivate the use of a feedback mechanism that adapts the excitation waveform to enforce the desired $J(t)$ shape. An example of such a sinusoidal $J(t)$ waveform is provided in Fig. 3, depicting a measurement at 100 Hz on a Ni–Fe ring sample prepared from a 500 µm sheet.

In this approach, the waveforms $H(t)$ and $J(t)$ are treated as parametric equations of the hysteresis loop. The iterative feedback procedure begins with a measurement using an initial excitation waveform (e.g., sinusoidal $H(t)$). Although the resulting loop corresponds to a distorted $J(t)$, it provides sufficient data to construct a new $H(t)$ waveform that yields the desired $J(t)$. The excitation signal $e(t)$ applied to the arbitrary waveform generator is derived using the primary circuit equation shown in Fig. 1. Assuming negligible air flux, this equation reads:

$$Ge(t) = u_R(t) + u_L(t) = (R_\mathrm{s} + R_H)i_H(t) + N_1 A\frac{\mathrm{d}J}{\mathrm{d}t}, \tag{3}$$

where G is the gain of the power amplifier (PA in Fig. 1), $R_\mathrm{s} + R_H$ is the total resistance of the primary circuit, and A is the cross-sectional area of the sample.

If air flux is not negligible, the inductive term $u_L(t)$ in Eq. (3) must be modified to:

$$u_L(t) = N_1\left(A\frac{\mathrm{d}J}{\mathrm{d}t} + A_\mathrm{tot}\mu_0\frac{\mathrm{d}H}{\mathrm{d}t}\right), \tag{4}$$

where A_tot is the total area enclosed by the primary winding.

This process is iterated to refine $H(t)$ and $e(t)$ until the resulting $J(t)$ waveform matches the target waveform. As a convergence criterion, the deviation in waveform form factor is used.

An example of the feedback process is shown in Fig. 4, demonstrating how the $J(t)$ distortion is eliminated after three iterations during measurements on a Ni–Fe sheet at $f =$ 100 Hz and $J_\mathrm{p} = 0.6$ T. The form factor of the final waveform reaches 1.110, which is within 0.1% of the theoretical sinusoidal value. Typically, only a few iterations (2–4) are required to achieve a desired waveform with form factor deviation within 0.2%–0.5%.

This digital feedback method is general and can be applied to synthesize various induction waveforms—such as square

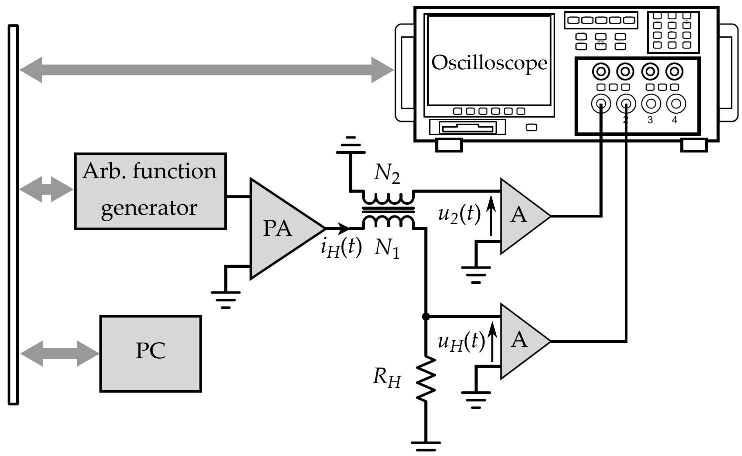

FIG. 1. Configuration of the wideband hysteresisgraph-wattmeter employed in the frequency range quasi-DC–1 MHz, incorporating digital feedback control to enforce a prescribed induction waveform.

FIG. 2. Hysteresisgraph-wattmeter built in the "Prof. Potocký Laboratory of Ferromagnetism".

or triangular—often required to simulate operational conditions in magnetic core applications. The accuracy and speed of convergence of this method are influenced by the resistive-reactive balance in the primary circuit. Optimal performance is achieved when the resistive and reactive contributions to Eq. (3) are of similar magnitude.

In the case of complex induction waveforms–such as those required to emulate application–specific operating conditions resulting in the formation of minor hysteresis loops—the feedback approach described previously becomes insufficient. To accommodate such conditions, a more general feedback algorithm was implemented. This method involves the iterative computation of a new excitation voltage $e(t)$ for the arbitrary waveform generator at the $(k+1)$-th iteration, given by:

$$e_{k+1}(t) = e_k(t) + \alpha\left[B_{\mathrm{ref}}(t) - B_k(t)\right] + \beta\left[\frac{\mathrm{d}B_{\mathrm{ref}}(t)}{\mathrm{d}t} - \frac{\mathrm{d}B_k(t)}{\mathrm{d}t}\right], \tag{5}$$

where B_{ref} is the desired induction waveform, α and β are appropriately small coefficients selected to ensure both sufficient convergence speed and suppression of undesired oscillatory behavior.

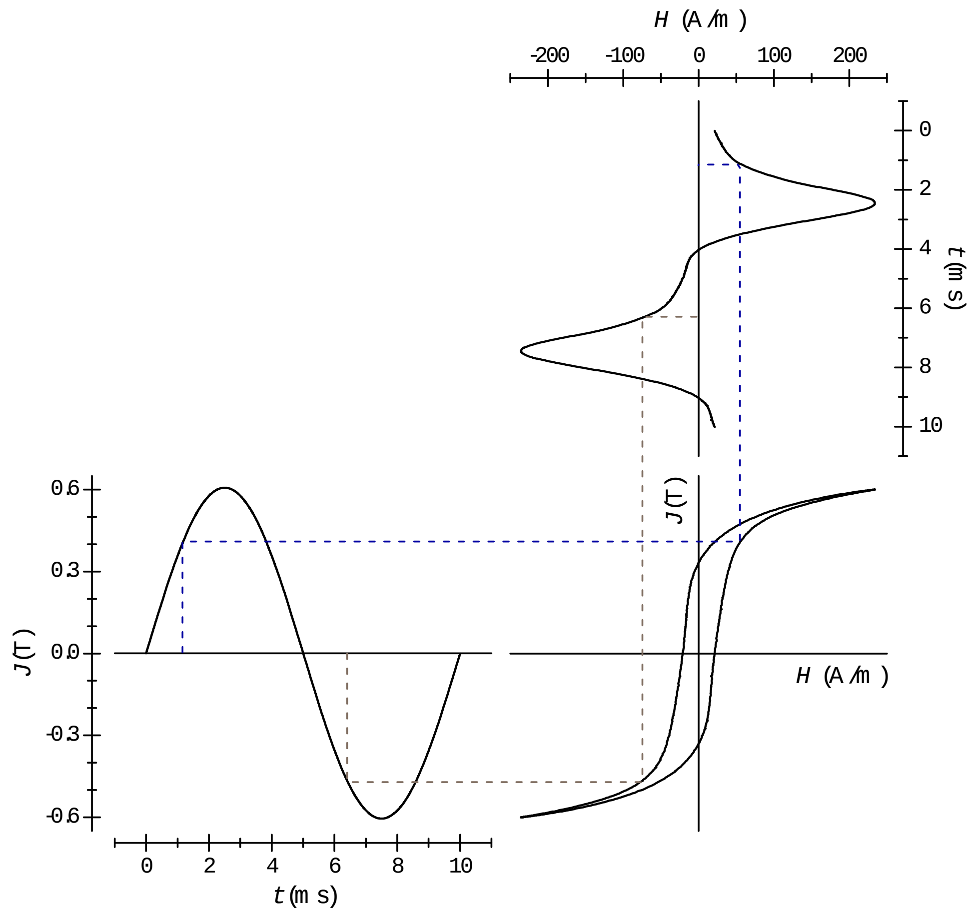

FIG. 3. Dynamic hysteresis loop of a ring sample cut from a 500 µm thick $Ni_{81}Fe_{19}$ sheet, measured at $f = 100$ Hz and $J_p = 0.6$ T. The H and J waveforms were controlled using digital feedback to impose a sinusoidal $J(t)$ waveform.

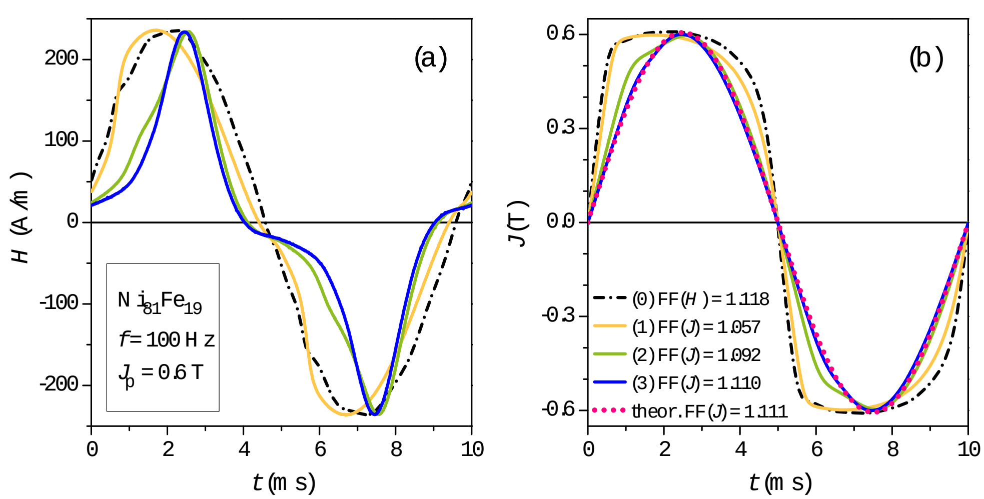

FIG. 4. Digital feedback enforcing a sinusoidal $J(t)$ waveform (b) through iterative refinement of the applied arbitrary $H(t)$ waveform (a). Measurements were performed on stacked rings made from 500 µm thick $Ni_{81}Fe_{19}$ sheet. The third iteration achieves the target sinusoidal behavior of $J(t)$.